

GeoWorld: Unlocking the Potential of Geometry Models to Facilitate High-Fidelity 3D Scene Generation

Yuhao Wan^{*1,2}, Lijuan Liu², Jingzhi Zhou¹, Zihan Zhou³, Xuying Zhang¹, Dongbo Zhang², Shaohui Jiao², Qibin Hou^{†1}, Ming-Ming Cheng¹

¹VCIP, School of Computer Science, Nankai University

²ByteDance Inc.

³Renmin University of China

^{*}Intern at ByteDance Inc. [†]Corresponding author.

Abstract: Previous works leveraging video models for image-to-3D scene generation tend to suffer from geometric distortions and blurry content. In this paper, we renovate the pipeline of image-to-3D scene generation by unlocking the potential of geometry models and present our **GeoWorld**. Instead of exploiting geometric information obtained from a single-frame input, we propose to first generate consecutive video frames and then take advantage of the geometry model to provide full-frame geometry features, which contain richer information than single-frame depth maps or camera embeddings used in previous methods, and use these geometry features as geometrical conditions to aid the video generation model. To enhance the consistency of geometric structures, we further propose a geometry alignment loss to provide the model with real-world geometric constraints and a geometry adaptation module to ensure the effective utilization of geometry features. Extensive experiments show that our GeoWorld can generate high-fidelity 3D scenes from a single image and a given camera trajectory, outperforming prior methods both qualitatively and quantitatively.

Project Page: <https://peaes.github.io/GeoWorld/>

HVision@Nankai

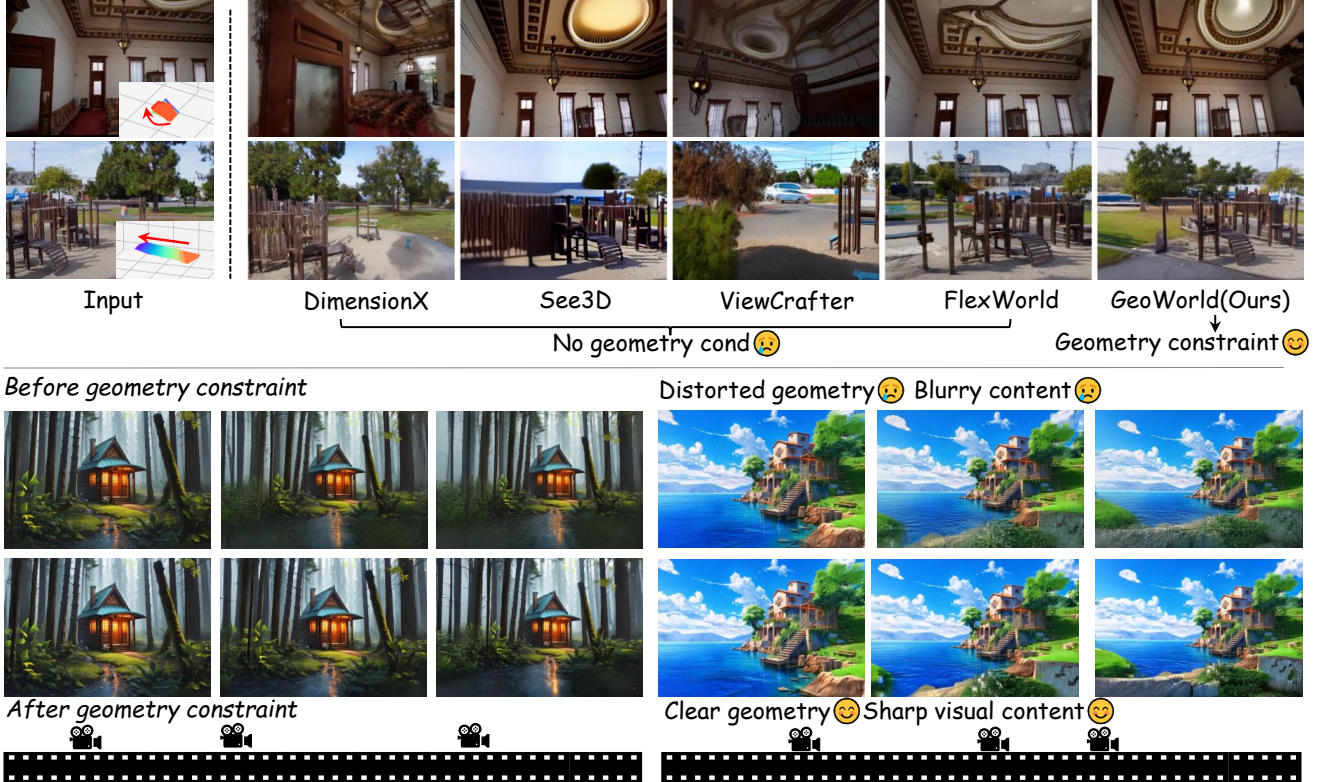


Figure 1 Visual comparisons. Top: Comparison between our **GeoWorld** and previous methods. By incorporating geometry constraints, our approach achieves superior visual quality. Bottom left: Results before applying geometry constraints, which often suffer from geometric distortions and blurry content. Bottom right: Results after applying geometry constraints. By unlocking the potential of geometry models, our **GeoWorld** produces clear geometric structures and sharp visual details.

1 Introduction

Generating a high-fidelity 3D scene from a single image has become a significant topic in recent years due to its high value in applications such as entertainment, interior and architectural design, and autonomous driving [9, 8, 23, 10, 56, 58, 47]. Leveraging deep learning methods for this task can significantly advance traditional 3D modeling pipelines. Given the limited information contained in a single image, a common approach is to utilize the generative priors of generative models to synthesize the scene content. Early methods [53, 32, 5, 59, 24, 4, 48, 14] often rely on 2D generative models [33, 13], which often lead to issues such as structural inconsistency and inconsistencies within the scene content.

Thanks to the advances in foundational 3D generative models, some recent works [50, 34, 3, 17, 51, 29] use video models [15, 46, 37] and leverage their implicit 3D priors to alleviate the aforementioned issues. Such methods typically employ video models to synthesize a video under a specified camera trajectory from a single input image, and subsequently reconstruct a 3D scene from the generated video. However, generating high-fidelity videos from a single image remains challenging. As shown at the top of Fig. 1, these methods tend to suffer from geometric distortions and blurry content that degrade the final 3D reconstruction quality. To address the above issues, a common approach is to provide additional geometry information for the model. As shown in Fig. 2(a), some previous works have utilized estimated monocular depth maps as spatial priors or camera embeddings to assist in video generation. Since these conditions essentially represent distilled 3D information, they inevitably introduce biases.

In this paper, we propose leveraging geometry models [38] to provide high-quality geometry conditions. These models inherently encode rich geometric information that captures a holistic understanding of the scene, providing a more complete representation than depth maps or camera embeddings. By taking advantage of the geometry models, we rethink the pipeline of image-to-3D scene generation and renovate the way of generating geometrical conditions. To be specific, we first render the single-frame input using the given camera trajectory. The resulting rendered partial views are fed into a fine-tuned video model to generate a coarse but content-complete video. This video can then be used as input to a geometry model to extract full-frame geometry features, providing reliable guidance for video generation.

Since the geometric information is derived from a model of limited accuracy, we further design a geometry alignment loss to compensate for this limitation beyond directly embedding the obtained geometry features as conditions, which aligns the geometry features extracted from the predicted video and the ground-truth video during training. This design implicitly provides the model with real-world geometric constraints, and the number of frames is naturally consistent. Finally, we propose a geometry adaptation module to effectively exploit the

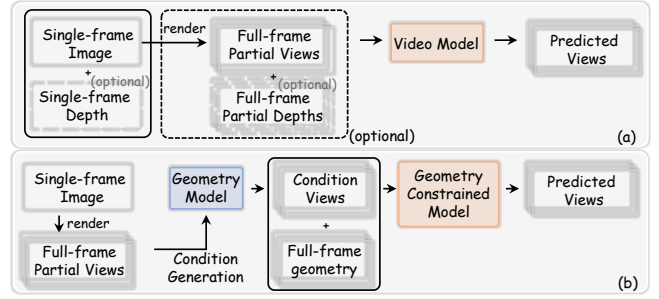


Figure 2 Pipeline comparison. (a) Pipelines of previous methods. Although details vary, their video models are conditioned only on single-frame information and limited geometric information. (b) Our GeoWorld leverages the geometrical condition generation procedure and a geometry model to obtain full-frame geometry features.

extracted full-frame geometry features for improving video generation quality.

A simplified comparison of our method to prior works can be found in Fig. 2. From Fig. 1, we can see that our GeoWorld is able to generate a high-fidelity 3D scene from a single image and a given camera trajectory, outperforming other state-of-the-art methods. To sum up, our contributions can be summarized as follows.

- We propose GeoWorld, a novel method that can generate a high-fidelity 3D scene from a single image and a given camera trajectory.
- We explore how to leverage geometry models to assist the video generation process. In this exploration, we design a geometrical condition generation procedure, a geometry alignment loss, and a geometry adaptation module to gradually unlock the potential of geometric information.
- Our GeoWorld outperforms all previous methods in both qualitative and quantitative comparisons, demonstrating the effectiveness of our method.

2 Related work

2.1 3D Scene Generation

Existing scene generation methods can be broadly categorized into four types. The first category comprises view-by-view image inpainting approaches [21, 49, 31, 48, 4, 59, 25, 45], which generate frames sequentially along a predefined camera trajectory. However, due to the lack of global semantic consistency, they struggle to produce semantically coherent full-scene results. The second category directly generates 3D scene representations [2, 26, 52, 35, 27] such as 3D Gaussian Splatting (3DGS) [19]. While these methods offer advantages in 3D consistency and reconstructability, their performance is often constrained by the scarcity of high-quality 3D data, posing challenges for training robust models. The third category

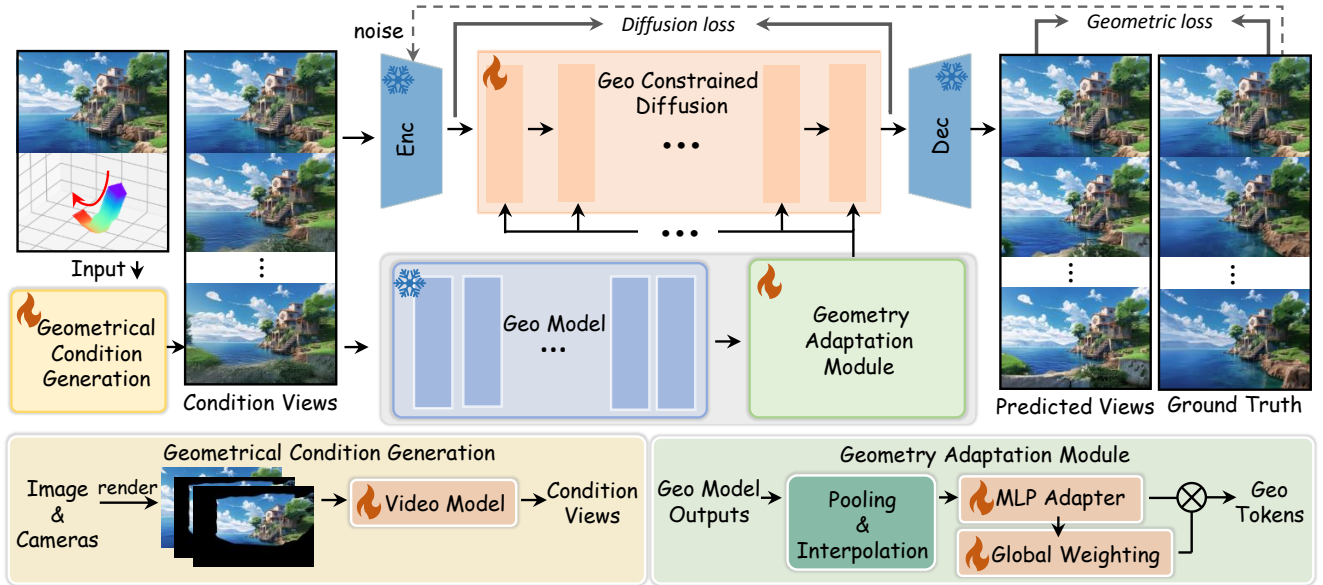


Figure 3 Overview of our GeoWorld. During training, we perform the geometrical condition generation procedure, feeding the obtained condition views into the geometry model to obtain full-frame geometry features, which are then processed by the geometry adaptation module. The condition views and the geometry features together serve as input to the geometry-constrained diffusion model to embed the geometric information. The predicted views produced by this model are then used to reconstruct the 3DGS scene.

is compositional scene generation [6, 18, 41, 47, 1], where the key idea is to generate individual objects and place them plausibly within a scene layout. Although significant progress has been made in 3D object generation, these methods still face unresolved issues related to model stability, object placement, and occlusion handling. The final category is controllable video generation [30, 50, 34, 3, 29, 57, 11], which aims to synthesize a sequence of spatially consistent video frames given a camera trajectory. This is typically achieved by fine-tuning pre-trained video diffusion models, which can produce visually appealing videos. However, such methods often exhibit geometric inconsistencies and structural artifacts that degrade the quality of subsequent 3D reconstructions.

To overcome these limitations, our method leverages multi-frame geometric information and introduces constraints to enforce spatial consistency, leading to highly competitive reconstruction results.

2.2 Learning-Based 3D Reconstruction

Unlike traditional 3D reconstruction pipelines that require training separately for each individual scene, learning-based reconstruction methods leverage neural networks trained on large-scale scene datasets to encode strong scene priors, ultimately achieving impressive open-world generalization capabilities [39, 40, 22, 38, 44, 42, 55]. DUST3R [40] directly regresses a 3D point cloud from a pair of RGB images. It extracts features from the two views using a transformer architecture enhanced with cross-attention mechanisms, and then feeds the fused features into a regression head to predict

the point cloud along with a confidence map. Its successor, MAST3R [22], maintains the two-view regression paradigm but introduces a confidence-weighted loss to improve prediction reliability. Recent methods have generalized the two-view alignment-based architecture to handle multi-view scenarios, allowing for the joint processing of long frame sequences—up to 100 frames or more—as demonstrated by models such as Fast3R [44] and VGGT [38]. VGGT scales up the core idea of DUST3R into a 1.2B-parameter transformer that jointly predicts camera intrinsics and extrinsics, dense depth maps, 3D point clouds, and 2D tracking features. The features extracted by such architectures exhibit strong 3D consistency and can support a wide range of downstream 3D tasks. Since video generation models often lack explicit 3D consistency control, introducing geometry features to guide the video generation process emerges as a natural and promising direction.

3 Methodology

As mentioned in Sec. 1, our goal is to leverage geometry models to provide reliable conditional signals for the video generation process. The overall architecture of our GeoWorld is shown in Fig. 3. Our design consists of three components: a geometrical condition generation procedure to obtain full-frame geometry features, a geometry alignment loss to introduce real-world geometric constraints, and a geometry adaptation module to utilize the geometry features effectively. For the video generation process, during training, we first fine-tune a video model. We then let this model perform inference

on the entire training set, and the newly generated data is used to train the geometry-constrained diffusion model. Finally, we use the predicted views to reconstruct the 3DGS scene.

3.1 Geometrical Condition Generation

The primary challenge of utilizing geometry models to help the video generation process lies in obtaining suitable geometry features. With only a single input frame, one can extract geometry for that frame alone, which provides limited guidance for subsequent frames in the video. We solve this by introducing a geometrical condition generation procedure to attain appropriate full-frame geometry features. As shown in Fig. 3, this procedure employs a fine-tuned video model to generate conditional views from the single-frame input and the given camera trajectory. In the full GeoWorld pipeline, these conditional views are then processed by the geometry model to obtain full-frame geometry features. Specifically, the entire process consists of two components: rendering and completion.

Rendering. The goal of this component is to obtain a video, in which each frame is the rendering of the input single-frame image under the given camera trajectory. This video serves as the input to the video model. The rendering procedure differs between the training and inference phases to ensure higher-quality inputs during training. During training, we reconstruct the 3DGS scene using all available frames from the dataset, and then start from a random frame, extract its depth from the 3DGS, and perform back-projection and pairing process [3]. During inference, we directly estimate the point cloud of the single-frame input under the given camera trajectory using MAST3R [22], and then perform back-projection.

Completion. The goal of this component is to use the fine-tuned video model to complete the rendered video into a content-complete one. Specifically, we first collect a batch of training data to fine-tune the video model directly. Then, the fine-tuned video model performs inference on the entire training dataset, and the newly generated data is used to train the geometry-constrained diffusion model shown in Fig. 3. In terms of model design, since only single-frame geometry features are available at this stage, we simply use them as additional conditions and embed them into the model through cross-attention.

Through this process, we can obtain full-frame geometry features with the help of the geometry model. These outcomes also reflect, to some extent, the limitations of directly fine-tuning video models for geometrically consistent video generation. In Sec. 4.3, we further discuss the quality of the conditional views (Fig. 8) and validate the role of the geometry features in the subsequent optimization process through comparisons (Fig. 7).

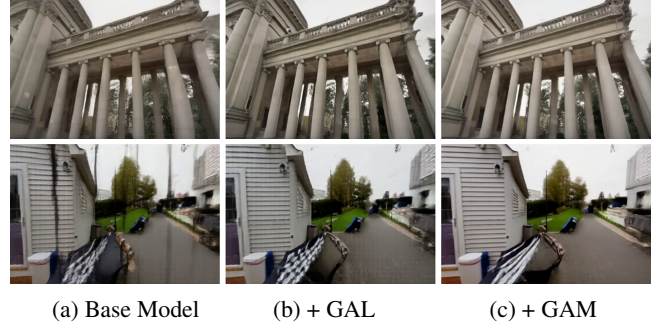


Figure 4 Visual comparisons of the design of the geometry-constrained diffusion model. Base model refers to directly embedding the geometry features into the model via cross-attention. ‘GAL’: geometry alignment loss. ‘GAM’: geometry adaptation module.

3.2 Geometry Alignment Loss

Although the geometrical condition generation process provides relatively complete geometric information, it is derived from a model of limited accuracy. To compensate for this limitation, we introduce real-world geometric information to guide the video generation process toward geometrically 3D scene synthesis. Specifically, we incorporate a geometry alignment loss into the diffusion objective, which compares the geometric features extracted from the generated and ground-truth videos. The loss is computed as the mean squared error between the two corresponding features obtained from the geometry model. In GeoWorld, this geometry model corresponds to the aggregator module of VGGT [38], with the decoding stage omitted to preserve complete geometric representations.

Specifically, given the ground-truth data I , a randomly sampled timestep t , and the corresponding Gaussian noise ϵ , we first encode I using the pre-trained VAE encoder and apply the forward process to obtain the input \mathbf{x} for the geometry-constrained diffusion model. Geometry tokens c_{geo} are obtained as described in Sec. 3.3. The diffusion loss is then defined as:

$$\mathcal{L}_{diff} = \mathbb{E}_{t, \epsilon \sim \mathcal{N}} \left[\|\epsilon - \epsilon_{\theta}(\mathbf{x}, c_{geo}, t)\|_2^2 \right]. \quad (1)$$

Given the predicted views I_{pred} and the geometry model G , the geometric loss is defined as:

$$\mathcal{L}_{geo} = \|G(I) - G(I_{pred})\|_2^2. \quad (2)$$

By leveraging the priors of the geometry model, this design could implicitly provide the model with real-world geometric information, ensuring that the optimization direction of the geometry-constrained model is geometrically consistent with the ground truth. The geometry alignment loss is defined as:

$$\mathcal{L} = \mathcal{L}_{diff} + \lambda \mathcal{L}_{geo}, \quad (3)$$

where λ is used as the weight for the geometric loss. As shown in Fig. 4, we observe that the outputs exhibit fewer geometric distortions and artifacts after incorporating the geometry alignment loss.

3.3 Geometry Adaptation Module

The goal of this subsection is to enable the model to effectively utilize the geometry features. In the latent space, since the output g of the geometry model differs from the input \mathbf{x} of the video model along the frame, height, and width dimensions, we first perform pooling along the frame dimension and interpolation along the height and width dimensions to obtain g_{resize} , aligning its size with \mathbf{x} . We then train an MLP-based adapter to process the resized features and align them with the latent space of the video model, resulting in g_{ada} .

Since the generation of condition views lacks geometric guidance, some regions inevitably exhibit ambiguous geometric structures. To prevent these ambiguous structures from misleading the model, we perform a global weighting on g_{ada} after processing it with the MLP adapter. We use an MLP-based predictor to integrate global information, similar to the Squeeze-and-Excitation block proposed in [16], and output a global weight for each token. By visualizing the global weights, we observe that low-weight tokens contain limited useful geometric information (Sec. 4.3). As a result, we multiply the global weights with g_{ada} and empirically discard the bottom 50% of tokens with lower weights to achieve a better performance, resulting in the final geometry tokens c_{geo} .

Finally, we fuse the obtained c_{geo} with \mathbf{x} using a single-frame cross-attention in each layer. Given the query Q from \mathbf{x} , key K from c_{geo} , and value V from c_{geo} , the formulation can be written as follows:

$$CA(Q, K, V) = \text{Softmax} \left(\frac{QK^T}{\sqrt{d_k}} + B \right) V, \quad (4)$$

where B is an aligned relative position embedding and $\sqrt{d_k}$ is a scaling factor as defined in [7].

4 Experiments

4.1 Experimental Settings

Model and training details. We use Wan2.1-1.3B [37] as our video model. During training, we set the batch size, learning rate, input image resolution, video frame length, and the weight for the geometric loss to 16, 5e-5, 192×336, 17, and 0.2, respectively. The video model in the geometrical condition generation procedure and the geometry-constrained model are trained for 7000 and 2000 iterations, respectively. The training process is conducted on 8 NVIDIA A100 GPUs.

Training Dataset. We use DL3DV [28] as our training dataset and construct training pairs following the dataset construction method proposed in FlexWorld [3] (See Sec. 3.1). Specifically, we sample two epochs from DL3DV and select the top 25% of cases with the smallest average camera translation and rotation, resulting in approximately 5000 video pairs.

Testing and evaluation. We use the RealEstate10K (RE10K) [60] and the Tanks and Temples (Tanks) [20] as our test datasets, following the same construction method as FlexWorld. We randomly select 100 video clips from RE10K and 100 video clips from Tanks, each of which consists of 49 frames. We adopt PSNR, SSIM [43], LPIPS [54], FID [12], and FVD [36] as our evaluation metrics.

4.2 Comparisons with State-of-the-Art Methods

Quantitative comparisons. We show the quantitative comparisons between our GeoWorld and recent state-of-the-art methods (DimensionX [34], See3D [30], ViewCrafter [50], and FlexWorld [3]) in Tab. 1 and Tab. 2. Tab. 1 reports the quantitative comparisons in novel view synthesis (i.e., the video generation process). We obtain the input of the video model following the method described in Sec. 3.1. As shown, our GeoWorld outperforms previous methods in terms of fidelity (PSNR, SSIM) and achieves competitive perceptual quality (LPIPS, FID, and FVD). In particular, the LPIPS score is lower than those of all previous methods, while the FID and FVD scores are only slightly higher than FlexWorld [3].

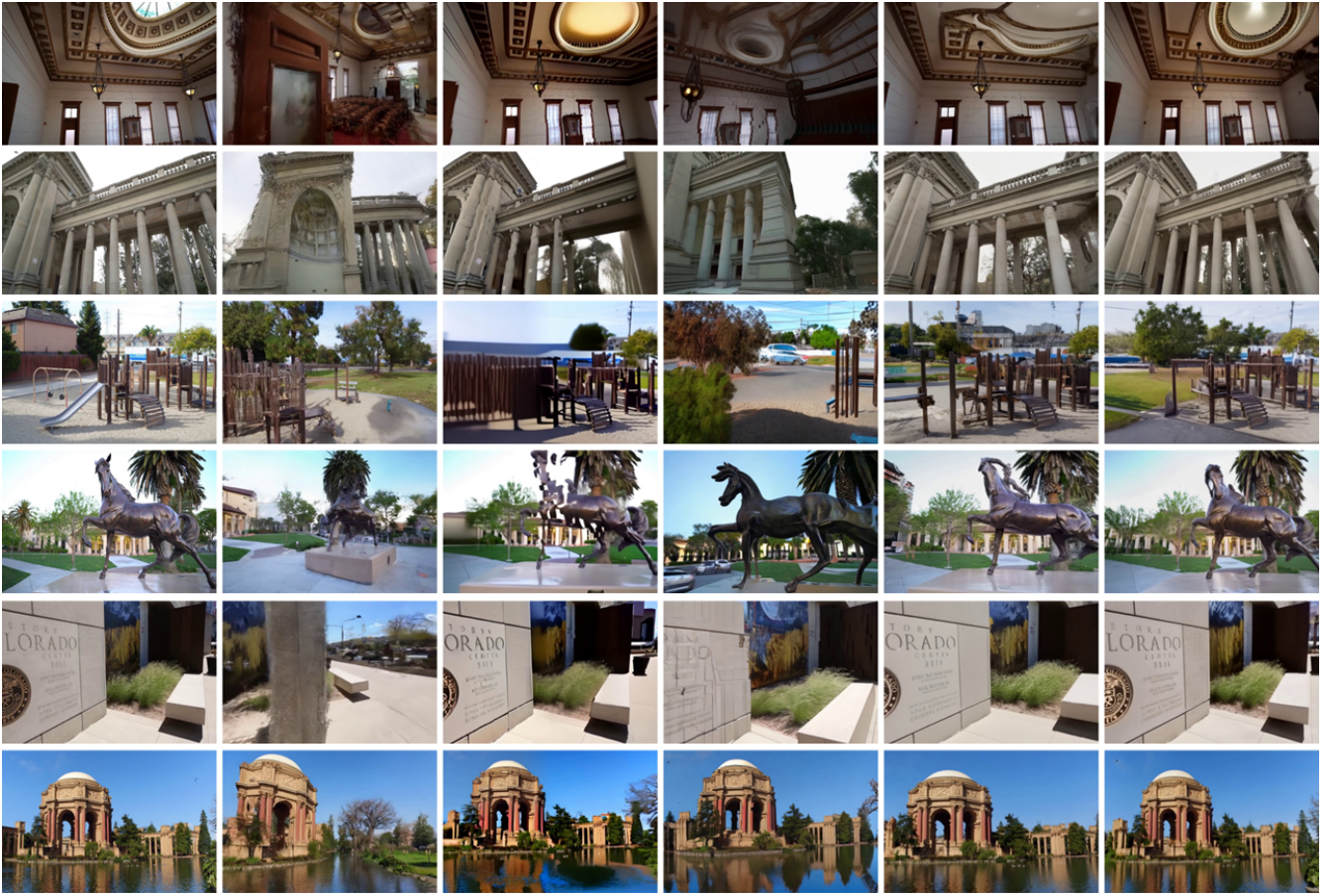
Tab. 2 presents the quantitative comparisons in 3D scene generation. We reconstruct the generated videos into 3DGS and render images from corresponding camera poses to compute the evaluation metrics. As shown, our GeoWorld surpasses previous methods across all metrics, including fidelity (PSNR, SSIM) and perceptual quality (LPIPS). All these results demonstrate the effectiveness of our method.

Qualitative comparisons. Fig. 5 and Fig. 6 show the qualitative comparison results. Fig. 5 presents the qualitative comparisons in novel view synthesis (i.e., the video generation process). As shown, the videos generated by our GeoWorld contain fewer artifacts, richer details, and exhibit stable camera control. Fig. 6 shows the qualitative comparisons in 3D scene generation. As illustrated, our GeoWorld can maintain high-quality geometric structures, while producing fewer artifacts compared to previous methods.

4.3 Ablation Study

Effectiveness of geometry constraints. We first evaluate the effectiveness of the geometric constraints by comparing the quality of the condition views produced by the geometrical condition generation procedure with predicted views produced by the geometry-constrained diffusion model. Fig. 7 shows the visual comparisons. It can be clearly observed that the refined videos contain almost no blurry regions, the generated objects are sharper, more detailed, and exhibit clearer geometric structures, demonstrating the effectiveness of geometric constraints.

Design of the geometry-constrained diffusion model. We then verify the rationality of our model design. The de-



(a) Ground Truth (b) DimensionX [34] (c) See3d [30] (d) ViewCrafter [50] (e) FlexWorld [3] (f) GeoWorld (ours)

Figure 5 Qualitative comparison of GeoWorld with state-of-the-art methods on **novel view synthesis**.

Table 1 Quantitative comparison of our GeoWorld with recent state-of-the-art methods on **novel view synthesis**. The best performances are in **bold** and the second performances are underlined.

Datasets	Method	PSNR \uparrow	SSIM \uparrow	LPIPS \downarrow	FID \downarrow	FVD \downarrow
RealEstate10K	DimensionX [34]	11.98	0.4579	0.6177	52.19	772.6
	See3D [30]	<u>14.60</u>	<u>0.5307</u>	<u>0.4402</u>	38.25	378.4
	ViewCrafter [50]	14.37	0.4854	0.4670	32.35	445.1
	FlexWorld [3]	14.28	0.5223	0.4418	30.56	270.4
	GeoWorld (ours)	17.28	0.6193	0.3297	<u>31.00</u>	<u>311.7</u>
Tanks and Temples	DimensionX [34]	11.57	0.3464	0.6200	55.73	1065
	See3D [30]	<u>13.00</u>	<u>0.3977</u>	<u>0.5400</u>	53.36	571.9
	ViewCrafter [50]	12.53	0.3651	0.5558	41.33	716.3
	FlexWorld [3]	12.99	0.3938	0.5298	38.69	422.6
	GeoWorld (ours)	14.99	0.4625	0.4556	<u>39.39</u>	<u>507.9</u>

Table 2 Quantitative comparison of our GeoWorld with recent state-of-the-art methods on **3D scene generation**.

Method	RealEstate10K			Tanks and Temples		
	PSNR \uparrow	SSIM \uparrow	LPIPS \downarrow	PSNR \uparrow	SSIM \uparrow	LPIPS \downarrow
DimensionX [34]	11.70	0.4205	0.6663	11.45	0.3192	0.6683
See3D [30]	<u>14.67</u>	<u>0.5315</u>	<u>0.4413</u>	<u>13.14</u>	<u>0.3979</u>	<u>0.5420</u>
FlexWorld [3]	13.71	0.4775	0.5174	12.46	0.3543	0.5785
GeoWorld (ours)	16.64	0.5970	0.4284	15.00	0.4642	0.5058

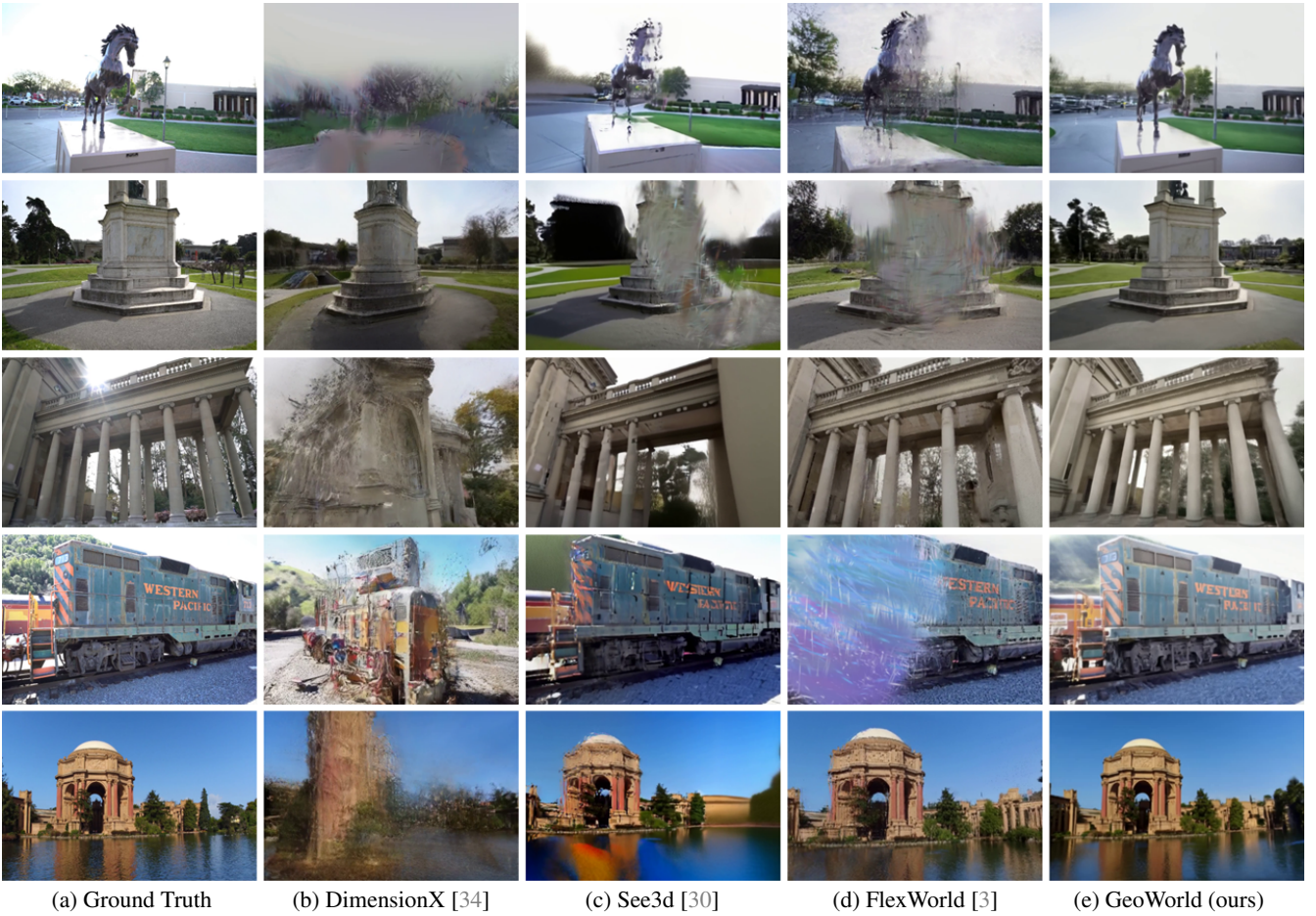


Figure 6 Qualitative comparison of our GeoWorld with recent stage-of-the-art methods on **3D scene generation**.

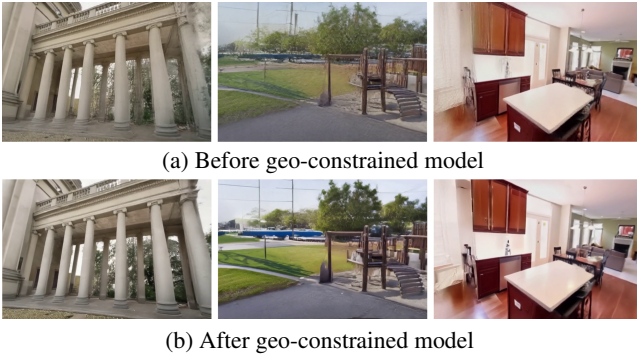


Figure 7 Visual comparisons of the geometry constraints.

sign of the geometry-constrained diffusion model consists of two main components: the geometry alignment loss described in Sec. 3.2 and the geometry adaptation module described in Sec. 3.3. The quantitative comparison results on the RE10K [60] test set are presented in Tab. 3. Base model refers to directly embedding the geometry features into the model via cross-attention. As shown, each component of our model contributes to improvements in the PSNR metric. In particular, introducing the geometry alignment loss leads to

Table 3 Design of geometry-constrained diffusion model.

Model	PSNR \uparrow	LPIPS \downarrow
Base Model	16.77 (+0.00)	0.3381 (+0.0000)
+Geometry Alignment Loss	16.96 (+0.19)	0.3284 (-0.0097)
<i>+Geometry Adaptation Module</i>		
+Resize	17.17 (+0.40)	0.3286 (-0.0095)
+Global Weighting	17.28 (+0.51)	0.3292 (-0.0089)

an improvement in the LPIPS metric, indicating enhanced perceptual quality, which is consistent with our objective of incorporating real-world geometric information. We also provide visual comparisons in Fig. 4. It can be observed that after introducing the geometry alignment loss, the distorted geometry and artifacts in the outputs are notably reduced, and further incorporating the geometry adaptation module leads to clearer geometric structures in the outputs.

Discussion about the geometrical condition generation procedure. The geometrical condition generation procedure in our overall pipeline requires additional discussion, mainly concerning the performance of the video model fine-tuned during this process. If the fine-tuned video model is under-

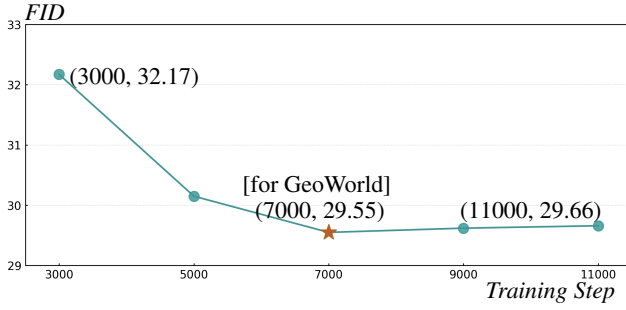


Figure 8 Quantitative comparisons of the geometrical condition generation procedure.

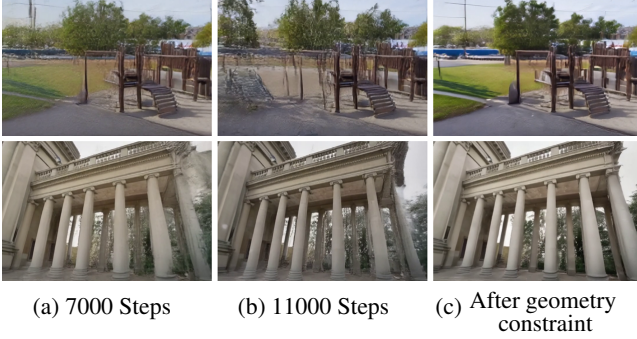


Figure 9 Visual comparisons of the geometrical condition generation procedure.

trained, it may fail to provide sufficient geometric information and could even introduce incorrect guidance to the geometry-constrained model. If the fine-tuned video model is trained for a sufficiently long time and can already generate highly detailed videos, the subsequent refinement process would become unnecessary. The results presented in Fig. 8 and Fig. 9 might address these concerns. As shown in Fig. 8, the model trained for 7000 steps achieves the lowest FID, and further increasing the training steps does not lead to additional improvements. The visual comparisons in Fig. 9 show that the fine-tuned video model (7000 steps) in the geometrical condition generation procedure still suffers from geometric distortions and blurry content even after an additional 4000 training steps (11000 steps). In contrast, the geometry-constrained model (with an additional 2000 steps) produces videos with clearer geometry and sharper visual content.

Analysis of global weighting process. We analyze the global weighting process proposed in Sec. 3.3. Fig. 10 presents the visualization results. The first row shows the condition views provided by the geometrical condition generation procedure, while the darker regions in the second row visualize the bottom 50% low-weight tokens identified by the global weighting process. It can be observed that our global weighting process effectively filters out low-quality tokens. As illustrated in the first column, this process is able to detect blurry regions within the condition views. In the second and third columns, when the conditional views contain few blurry regions, the process tends to retain regions containing richer

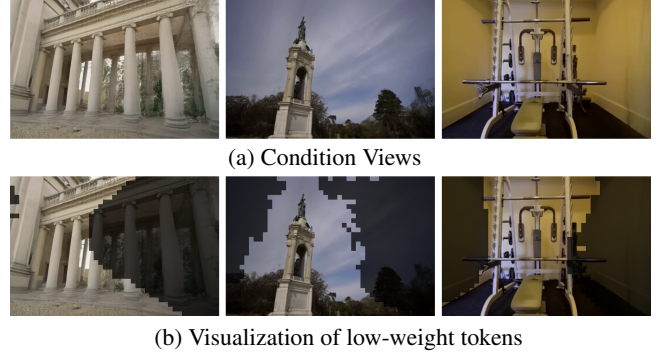


Figure 10 Visualization of the global weighting process. The darker regions in the second row visualize the bottom 50% low-weight tokens identified by the global weighting process.

geometric structures (e.g., the sky and plain-colored walls contain limited geometric information).

5 Conclusions

In this paper, we propose GeoWorld, a novel method that can generate a high-fidelity 3D scene from a single image. Our main advancement over previous works lies in effectively leveraging geometry models to improve the video generation process. We enable the model to obtain more reliable geometric information through the design of the overall pipeline and further introduce a geometry-constrained model to make efficient use of it. Extensive experiments demonstrate the effectiveness of our method, which outperforms all previous methods in both qualitative and quantitative comparisons. We expect that our GeoWorld can inspire future research and provide a new perspective for designing image-to-3D scene generation models.

References

- [1] Andreea Ardelean, Mert  zer, and Bernhard Egger. Gen3dsr: Generalizable 3d scene reconstruction via divide and conquer from a single view. In *2025 International Conference on 3D Vision (3DV)*, pages 616–626. IEEE, 2025. 3
- [2] Yuanhao Cai, He Zhang, Kai Zhang, Yixun Liang, Mengwei Ren, Fujun Luan, Qing Liu, Soo Ye Kim, Jianming Zhang, Zhifei Zhang, et al. Baking gaussian splatting into diffusion denoiser for fast and scalable single-stage image-to-3d generation and reconstruction. In *Proceedings of the IEEE/CVF International Conference on Computer Vision*, pages 25062–25072, 2025. 2
- [3] Luxi Chen, Zihan Zhou, Min Zhao, Yikai Wang, Ge Zhang, Wenhao Huang, Hao Sun, Ji-Rong Wen, and Chongxuan Li. Flexworld: Progressively expanding

- 3d scenes for flexible-view synthesis. *arXiv preprint arXiv:2503.13265*, 2025. 2, 3, 4, 5, 6, 7, 12, 15
- [4] Jaeyoung Chung, Suyoung Lee, Hyeongjin Nam, Jaerin Lee, and Kyoung Mu Lee. Lucidreamer: Domain-free generation of 3d gaussian splatting scenes. *arXiv preprint arXiv:2311.13384*, 2023. 2
- [5] Dana Cohen-Bar, Elad Richardson, Gal Metzer, Raja Giryes, and Daniel Cohen-Or. Set-the-scene: Global-local training for generating controllable nerf scenes. In *Proceedings of the IEEE/CVF International Conference on Computer Vision*, pages 2920–2929, 2023. 2
- [6] Wenqi Dong, Bangbang Yang, Zesong Yang, Yuan Li, Tao Hu, Hujun Bao, Yuewen Ma, and Zhaopeng Cui. Hiscene: creating hierarchical 3d scenes with isometric view generation. In *Proceedings of the 33rd ACM International Conference on Multimedia*, pages 9783–9792, 2025. 3
- [7] Alexey Dosovitskiy, Lucas Beyer, Alexander Kolesnikov, Dirk Weissenborn, Xiaohua Zhai, Thomas Unterthiner, Mostafa Dehghani, Matthias Minderer, Georg Heigold, Sylvain Gelly, et al. An image is worth 16x16 words: Transformers for image recognition at scale. *arXiv preprint arXiv:2010.11929*, 2020. 5
- [8] Ruiyuan Gao, Kai Chen, Enze Xie, Lanqing Hong, Zhenguo Li, Dit-Yan Yeung, and Qiang Xu. Magic-drive: Street view generation with diverse 3d geometry control. *arXiv preprint arXiv:2310.02601*, 2023. 2
- [9] Ruiqi Gao, Aleksander Holynski, Philipp Henzler, Arthur Brussee, Ricardo Martin-Brualla, Pratul Srivasan, Jonathan T Barron, and Ben Poole. Cat3d: Create anything in 3d with multi-view diffusion models. *arXiv preprint arXiv:2405.10314*, 2024. 2
- [10] Jiazhe Guo, Yikang Ding, Xiwu Chen, Shuo Chen, Bohan Li, Yingshuang Zou, Xiaoyang Lyu, Feiyang Tan, Xiaojuan Qi, Zhiheng Li, et al. Dist-4d: Disentangled spatiotemporal diffusion with metric depth for 4d driving scene generation. *arXiv preprint arXiv:2503.15208*, 2025. 2
- [11] Hao He, Yinghao Xu, Yuwei Guo, Gordon Wetzstein, Bo Dai, Hongsheng Li, and Ceyuan Yang. Cameractrl: Enabling camera control for text-to-video generation. *arXiv preprint arXiv:2404.02101*, 2024. 3
- [12] Martin Heusel, Hubert Ramsauer, Thomas Unterthiner, Bernhard Nessler, and Sepp Hochreiter. Gans trained by a two time-scale update rule converge to a local nash equilibrium. *Advances in neural information processing systems*, 30, 2017. 5
- [13] Jonathan Ho, Ajay Jain, and Pieter Abbeel. Denoising diffusion probabilistic models. *Advances in neural information processing systems*, 33:6840–6851, 2020. 2
- [14] Lukas Höllein, Ang Cao, Andrew Owens, Justin Johnson, and Matthias Nießner. Text2room: Extracting textured 3d meshes from 2d text-to-image models. In *Proceedings of the IEEE/CVF International Conference on Computer Vision*, pages 7909–7920, 2023. 2
- [15] Wenyi Hong, Ming Ding, Wendi Zheng, Xinghan Liu, and Jie Tang. Cogvideo: Large-scale pretraining for text-to-video generation via transformers. *arXiv preprint arXiv:2205.15868*, 2022. 2
- [16] Jie Hu, Li Shen, and Gang Sun. Squeeze-and-excitation networks. In *Proceedings of the IEEE conference on computer vision and pattern recognition*, pages 7132–7141, 2018. 5
- [17] Tianyu Huang, Wangguandong Zheng, Tengfei Wang, Yuhao Liu, Zhenwei Wang, Junta Wu, Jie Jiang, Hui Li, Rynson WH Lau, Wangmeng Zuo, et al. Voyager: Long-range and world-consistent video diffusion for explorable 3d scene generation. *arXiv preprint arXiv:2506.04225*, 2025. 2
- [18] Zehuan Huang, Yuan-Chen Guo, Xingqiao An, Yunhan Yang, Yangguang Li, Zi-Xin Zou, Ding Liang, Xihui Liu, Yan-Pei Cao, and Lu Sheng. Midi: Multi-instance diffusion for single image to 3d scene generation. In *Proceedings of the Computer Vision and Pattern Recognition Conference*, pages 23646–23657, 2025. 3
- [19] Bernhard Kerbl, Georgios Kopanas, Thomas Leimkühler, and George Drettakis. 3d gaussian splatting for real-time radiance field rendering. *ACM Trans. Graph.*, 42(4):139–1, 2023. 2
- [20] Arno Knapitsch, Jaesik Park, Qian-Yi Zhou, and Vladlen Koltun. Tanks and temples: Benchmarking large-scale scene reconstruction. *ACM Transactions on Graphics (ToG)*, 36(4):1–13, 2017. 5
- [21] Jiabao Lei, Jiapeng Tang, and Kui Jia. Rgb2: Generative scene synthesis via incremental view inpainting using rgb2 diffusion models. In *Proceedings of the IEEE/CVF conference on computer vision and pattern recognition*, pages 8422–8434, 2023. 2
- [22] Vincent Leroy, Yohann Cabon, and Jérôme Revaud. Grounding image matching in 3d with mast3r. In *European Conference on Computer Vision*, pages 71–91. Springer, 2024. 3, 4
- [23] Bohan Li, Jiazhe Guo, Hongsi Liu, Yingshuang Zou, Yikang Ding, Xiwu Chen, Hu Zhu, Feiyang Tan, Chi Zhang, Tiancai Wang, et al. Uniscene: Unified occupancy-centric driving scene generation. In *Proceedings of the Computer Vision and Pattern Recognition Conference*, pages 11971–11981, 2025. 2
- [24] Haoran Li, Haolin Shi, Wenli Zhang, Wenjun Wu, Yong Liao, Lin Wang, Lik-hang Lee, and Peng Yuan Zhou.

- Dreamscene: 3d gaussian-based text-to-3d scene generation via formation pattern sampling. In *European Conference on Computer Vision*, pages 214–230. Springer, 2024. 2
- [25] Ming-Feng Li, Yueh-Feng Ku, Hong-Xuan Yen, Chi Liu, Yu-Lun Liu, Albert YC Chen, Cheng-Hao Kuo, and Min Sun. Genrc: Generative 3d room completion from sparse image collections. In *European Conference on Computer Vision*, pages 146–163. Springer, 2024. 2
- [26] Xinyang Li, Zhangyu Lai, Linning Xu, Yansong Qu, Lijuan Cao, Shengchuan Zhang, Bo Dai, and Rongrong Ji. Director3d: Real-world camera trajectory and 3d scene generation from text. *Advances in neural information processing systems*, 37:75125–75151, 2024. 2
- [27] Hanwen Liang, Junli Cao, Vidit Goel, Guocheng Qian, Sergei Korolev, Demetri Terzopoulos, Konstantinos N Plataniotis, Sergey Tulyakov, and Jian Ren. Wonderland: Navigating 3d scenes from a single image. In *Proceedings of the Computer Vision and Pattern Recognition Conference*, pages 798–810, 2025. 2
- [28] Lu Ling, Yichen Sheng, Zhi Tu, Wentian Zhao, Cheng Xin, Kun Wan, Lantao Yu, Qianyu Guo, Zixun Yu, Yawen Lu, et al. D13dv-10k: A large-scale scene dataset for deep learning-based 3d vision. In *Proceedings of the IEEE/CVF Conference on Computer Vision and Pattern Recognition*, pages 22160–22169, 2024. 5
- [29] Lijuan Liu, Wenfa Li, Dongbo Zhang, Shuo Wang, and Shaohui Jiao. Idcnet: Guided video diffusion for metric-consistent rgbd scene generation with precise camera control. *arXiv preprint arXiv:2508.04147*, 2025. 2, 3
- [30] Baorui Ma, Huachen Gao, Haoge Deng, Zhengxiong Luo, Tiejun Huang, Lulu Tang, and Xinlong Wang. You see it, you got it: Learning 3d creation on pose-free videos at scale. In *Proceedings of the Computer Vision and Pattern Recognition Conference*, pages 2016–2029, 2025. 3, 5, 6, 7, 12, 15
- [31] Yikun Ma, Dandan Zhan, and Zhi Jin. Fastscene: Text-driven fast 3d indoor scene generation via panoramic gaussian splatting. *arXiv preprint arXiv:2405.05768*, 2024. 2
- [32] Ben Poole, Ajay Jain, Jonathan T Barron, and Ben Mildenhall. Dreamfusion: Text-to-3d using 2d diffusion. *arXiv preprint arXiv:2209.14988*, 2022. 2
- [33] Robin Rombach, Andreas Blattmann, Dominik Lorenz, Patrick Esser, and Björn Ommer. High-resolution image synthesis with latent diffusion models. In *Proceedings of the IEEE/CVF conference on computer vision and pattern recognition*, pages 10684–10695, 2022. 2
- [34] Wenqiang Sun, Shuo Chen, Fangfu Liu, Zilong Chen, Yueqi Duan, Jun Zhang, and Yikai Wang. Dimensionx: Create any 3d and 4d scenes from a single image with controllable video diffusion. *arXiv preprint arXiv:2411.04928*, 2024. 2, 3, 5, 6, 7, 12, 15
- [35] Stanislaw Szymanowicz, Eldar Insafutdinov, Chuanxia Zheng, Dylan Campbell, Joao F Henriques, Christian Rupprecht, and Andrea Vedaldi. Flash3d: Feed-forward generalisable 3d scene reconstruction from a single image. *arXiv preprint arXiv:2406.04343*, 2024. 2
- [36] Thomas Unterthiner, Sjoerd Van Steenkiste, Karol Kurach, Raphaël Marinier, Marcin Michalski, and Sylvain Gelly. Fvd: A new metric for video generation. 2019. 5
- [37] Team Wan, Ang Wang, Baole Ai, Bin Wen, Chaojie Mao, Chen-Wei Xie, Di Chen, Feiwu Yu, Haiming Zhao, Jianxiao Yang, et al. Wan: Open and advanced large-scale video generative models. *arXiv preprint arXiv:2503.20314*, 2025. 2, 5
- [38] Jianyuan Wang, Minghao Chen, Nikita Karaev, Andrea Vedaldi, Christian Rupprecht, and David Novotny. Vggt: Visual geometry grounded transformer. In *Proceedings of the Computer Vision and Pattern Recognition Conference*, pages 5294–5306, 2025. 2, 3, 4
- [39] Qianqian Wang, Yifei Zhang, Aleksander Holynski, Alexei A Efros, and Angjoo Kanazawa. Continuous 3d perception model with persistent state. In *Proceedings of the Computer Vision and Pattern Recognition Conference*, pages 10510–10522, 2025. 3
- [40] Shuzhe Wang, Vincent Leroy, Yohann Cabon, Boris Chidlovskii, and Jerome Revaud. Dust3r: Geometric 3d vision made easy. In *Proceedings of the IEEE/CVF Conference on Computer Vision and Pattern Recognition*, pages 20697–20709, 2024. 3
- [41] Yian Wang, Xiaowen Qiu, Jiageng Liu, Zhehuan Chen, Jiting Cai, Yufei Wang, Tsun-Hsuan Johnson Wang, Zhou Xian, and Chuang Gan. Architect: Generating vivid and interactive 3d scenes with hierarchical 2d inpainting. *Advances in Neural Information Processing Systems*, 37:67575–67603, 2024. 3
- [42] Yifan Wang, Jianjun Zhou, Haoyi Zhu, Wenzheng Chang, Yang Zhou, Zizun Li, Junyi Chen, Jiangmiao Pang, Chunhua Shen, and Tong He. π^3 : Permutation-equivariant visual geometry learning. *arXiv preprint arXiv:2507.13347*, 2025. 3
- [43] Zhou Wang, Alan C Bovik, Hamid R Sheikh, and Eero P Simoncelli. Image quality assessment: from error visibility to structural similarity. *IEEE transactions on image processing*, 13(4):600–612, 2004. 5
- [44] Jianing Yang, Alexander Sax, Kevin J Liang, Mikael Henaff, Hao Tang, Ang Cao, Joyce Chai, Franziska Meier, and Matt Feiszli. Fast3r: Towards 3d reconstruction of 1000+ images in one forward pass. In *Proceedings of the Computer Vision and Pattern Recognition Conference*, pages 21924–21935, 2025. 3

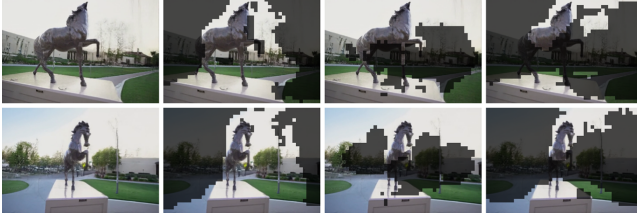
- [45] Shuai Yang, Jing Tan, Mengchen Zhang, Tong Wu, Gordon Wetzstein, Ziwei Liu, and Dahua Lin. Layerpano3d: Layered 3d panorama for hyper-immersive scene generation. In *Proceedings of the Special Interest Group on Computer Graphics and Interactive Techniques Conference Conference Papers*, pages 1–10, 2025. 2
- [46] Zhuoyi Yang, Jiayan Teng, Wendi Zheng, Ming Ding, Shiyu Huang, Jiazheng Xu, Yuanming Yang, Wenyi Hong, Xiaohan Zhang, Guanyu Feng, et al. Cogvideox: Text-to-video diffusion models with an expert transformer. *arXiv preprint arXiv:2408.06072*, 2024. 2
- [47] Kaixin Yao, Longwen Zhang, Xinhao Yan, Yan Zeng, Qixuan Zhang, Wei Yang, Lan Xu, Jiayuan Gu, and Jingyi Yu. Cast: Component-aligned 3d scene reconstruction from an rgb image. *arXiv preprint arXiv:2502.12894*, 2025. 2, 3
- [48] Hong-Xing Yu, Haoyi Duan, Charles Herrmann, William T Freeman, and Jiajun Wu. Wonderworld: Interactive 3d scene generation from a single image. In *Proceedings of the Computer Vision and Pattern Recognition Conference*, pages 5916–5926, 2025. 2
- [49] Hong-Xing Yu, Haoyi Duan, Junhwa Hur, Kyle Sargent, Michael Rubinstein, William T Freeman, Forrester Cole, Deqing Sun, Noah Snavely, Jiajun Wu, et al. Wonderjourney: Going from anywhere to everywhere. In *Proceedings of the IEEE/CVF Conference on Computer Vision and Pattern Recognition*, pages 6658–6667, 2024. 2
- [50] Wangbo Yu, Jinbo Xing, Li Yuan, Wenbo Hu, Xiaoyu Li, Zhipeng Huang, Xiangjun Gao, Tien-Tsin Wong, Ying Shan, and Yonghong Tian. Viewcrafter: Taming video diffusion models for high-fidelity novel view synthesis. *arXiv preprint arXiv:2409.02048*, 2024. 2, 3, 5, 6, 12, 15
- [51] Shangjin Zhai, Zhichao Ye, Jialin Liu, Weijian Xie, Jiaqi Hu, Zhen Peng, Hua Xue, Danpeng Chen, Xiaomeng Wang, Lei Yang, et al. Stargen: A spatiotemporal autoregression framework with video diffusion model for scalable and controllable scene generation. In *Proceedings of the Computer Vision and Pattern Recognition Conference*, pages 26822–26833, 2025. 2
- [52] Kai Zhang, Sai Bi, Hao Tan, Yuanbo Xiangli, Nanxuan Zhao, Kalyan Sunkavalli, and Zexiang Xu. Gs-lrm: Large reconstruction model for 3d gaussian splatting. In *European Conference on Computer Vision*, pages 1–19. Springer, 2024. 2
- [53] Qihang Zhang, Chaoyang Wang, Aliaksandr Siarohin, Peiye Zhuang, Yinghao Xu, Ceyuan Yang, Dahua Lin, Bolei Zhou, Sergey Tulyakov, and Hsin-Ying Lee. Towards text-guided 3d scene composition. In *Proceedings of the IEEE/CVF Conference on Computer Vision and Pattern Recognition*, pages 6829–6838, 2024. 2
- [54] Richard Zhang, Phillip Isola, Alexei A Efros, Eli Shechtman, and Oliver Wang. The unreasonable effectiveness of deep features as a perceptual metric. In *Proceedings of the IEEE conference on computer vision and pattern recognition*, pages 586–595, 2018. 5
- [55] Shangzhan Zhang, Jianyuan Wang, Yinghao Xu, Nan Xue, Christian Rupprecht, Xiaowei Zhou, Yujun Shen, and Gordon Wetzstein. Flare: Feed-forward geometry, appearance and camera estimation from uncalibrated sparse views. In *Proceedings of the Computer Vision and Pattern Recognition Conference*, pages 21936–21947, 2025. 3
- [56] Xuying Zhang, Yupeng Zhou, Kai Wang, Yikai Wang, Zhen Li, Shaohui Jiao, Daquan Zhou, Qibin Hou, and Ming-Ming Cheng. Ar-1-to-3: Single image to consistent 3d object via next-view prediction. In *Proceedings of the IEEE/CVF International Conference on Computer Vision*, pages 26273–26283, 2025. 2
- [57] Yuyang Zhao, Chung-Ching Lin, Kevin Lin, Zhiwen Yan, Linjie Li, Zhengyuan Yang, Jianfeng Wang, Gim Hee Lee, and Lijuan Wang. Genxd: Generating any 3d and 4d scenes. *arXiv preprint arXiv:2411.02319*, 2024. 3
- [58] Jensen Zhou, Hang Gao, Vikram Voleti, Aaryaman Vasishta, Chun-Han Yao, Mark Boss, Philip Torr, Christian Rupprecht, and Varun Jampani. Stable virtual camera: Generative view synthesis with diffusion models. *arXiv preprint arXiv:2503.14489*, 2025. 2
- [59] Shijie Zhou, Zhiwen Fan, Dejia Xu, Haoran Chang, Pradyumna Chari, Tejas Bharadwaj, Suyu You, Zhangyang Wang, and Achuta Kadambi. Dreamscene360: Unconstrained text-to-3d scene generation with panoramic gaussian splatting. In *European Conference on Computer Vision*, pages 324–342. Springer, 2024. 2
- [60] Tinghui Zhou, Richard Tucker, John Flynn, Graham Fyfe, and Noah Snavely. Stereo magnification: Learning view synthesis using multiplane images. *arXiv preprint arXiv:1805.09817*, 2018. 5, 7

A More Ablation Study

Ablation on the discard ratio in the global weighting process.

Table 4 Ablation on the discard ratio in the global weighting process.

Discard ratio	PSNR \uparrow	SSIM \uparrow
<i>For GeoWorld</i>		
50%	17.28 (+0.00)	0.6193 (+0.0000)
30%	17.17 (-0.11)	0.6173 (-0.0020)
70%	17.22 (-0.06)	0.6188 (-0.0005)



(a) Cond. Views (b) 50% (c) 30% (d) 70%

Figure 11 Visual comparisons of different discard ratios in the global weighting process. The darker regions visualize the discarded tokens.

In Tab. 4, we further present the effects of different discard ratios in the global weighting process. As shown, a ratio of 50% serves as the best practice. Both 30% and 70% lead to slight decreases in fidelity metrics (PSNR, SSIM). Fig. 11 presents the visualization of the discarded tokens. As shown, when the discard ratio is set to 30%, some low-quality regions (e.g., blurry content or regions that contain limited geometric information) are still retained. When the ratio increases to 70%, although most low-quality regions are effectively removed, a considerable portion of the geometrically informative main regions is also discarded. A discard ratio of 50% strikes a favorable balance between the two.

B More visual comparisons

More results of our GeoWorld. We present more results produced by our GeoWorld in Fig. 12 and Fig. 13. In addition, the supplementary material ZIP file includes extra results generated by GeoWorld using the same input image under different camera trajectories. Files “result1.mp4” through “result6.mp4” correspond to individual examples, while “GeoWorld_different_trajectory.mp4” is a concatenation of these samples. We believe that these results clearly demonstrate the generation capability of GeoWorld. Even under large viewpoint changes, our model is able to produce high-quality results.

More visual comparisons in novel view synthesis. We provide more visual comparisons in novel view synthesis in Fig. 14. As shown, compared with previous meth-

ods (DimensionX [34], See3d [30], ViewCrafter [50], and FlexWorld [3]), our GeoWorld produces results with fewer artifacts and clearer geometric structures.

More visual comparisons in 3D scene generation. We also provide more visual comparisons of 3D scene generation in Fig. 15. As shown, compared with previous methods (DimensionX [34], See3d [30], and FlexWorld [3]), our GeoWorld produces results with better geometric consistency, sharpness, and overall visual quality.

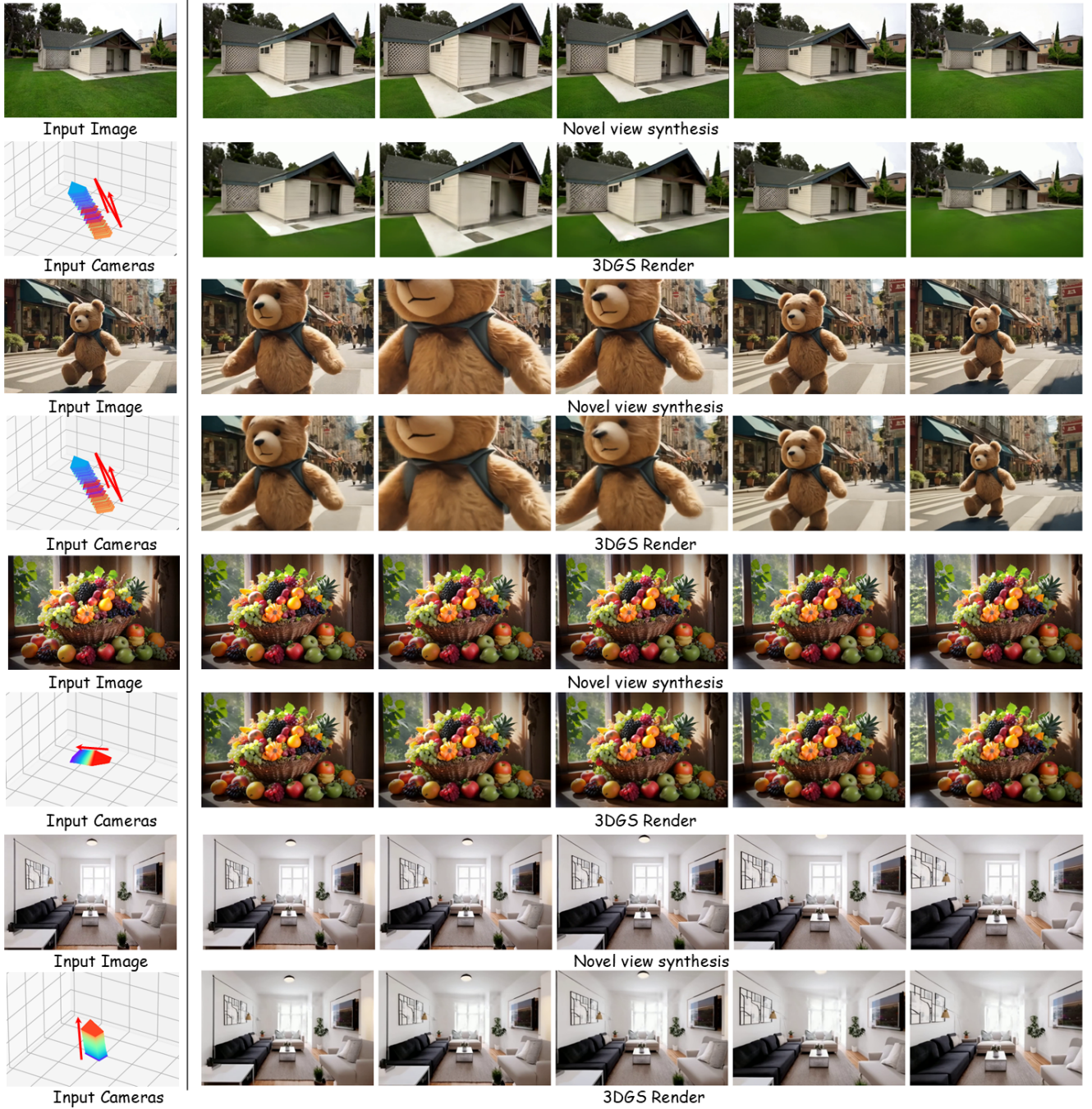


Figure 12 More results of our GeoWorld. Our GeoWorld is capable of producing high-quality videos under various camera trajectories. Thanks to the reliable geometric consistency across frames, the 3DGS renderings also show high-quality visual results.

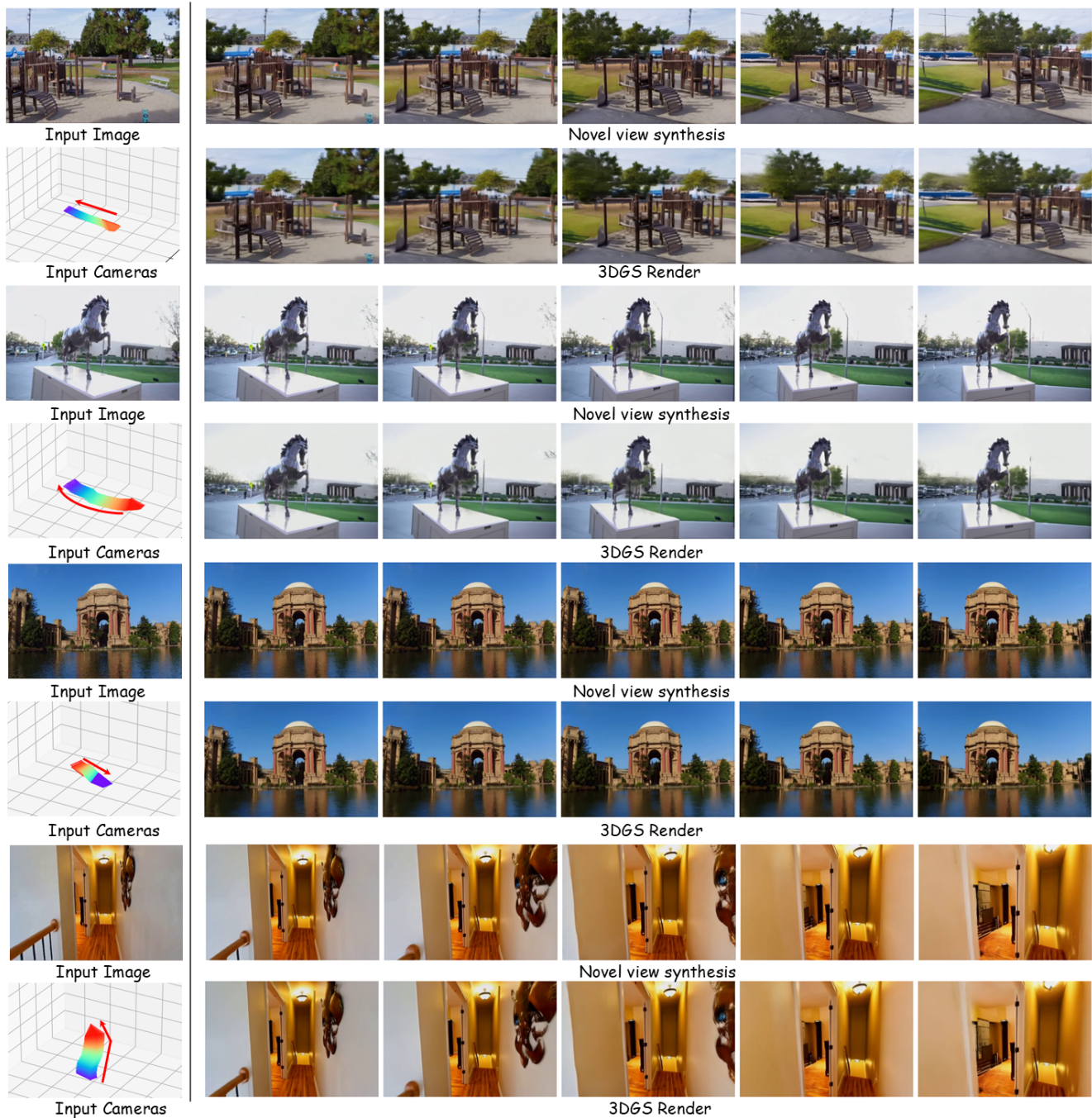


Figure 13 More results of our GeoWorld.



Figure 14 More visual comparisons of GeoWorld with state-of-the-art methods on **novel view synthesis**.



Figure 15 More visual comparisons of our GeoWorld with recent stage-of-the-art methods on **3D scene generation**.